Judd-Ofelt analysis, visible to NIR photoluminescence emission under 450 nm and 976 nm excitations and energy transfer of barium fluorotellurite glasses doping with Ho^{3+}, Yb^{3+}, Ho^{3+}:Yb^{3+}

E. Kumi-Barimah, Y. Chen, G. Sharma, A. Jha

The School of Chemical and Process Engineering, University of Leeds, Woodhouse Lane, Leeds, LS2 9JT, UK
corresponding author: e.kumi-barimah@leeds.ac.uk

Abstract

Barium fluorotellurite glasses doping with Ho^{3+}, Yb^{3+}, and Ho^{3+}:Yb^3 were fabricated using the conventional melt and quenching method, and their optical properties were studied using different optical spectroscopic techniques. The FITR absorption band at 3000 cm^{-1} was used to investigate OH- concentrations of the prepared glasses, which increased with Yb^{3+} content. However, it decreased by substituting a portion of BaF$_2$ content with Ba$_2$CO$_3$ concentration. The electric dipole line strengths and Judd-Ofelt parameters were estimated using UV-visible-near infrared (NIR) optical absorption spectra to gain information on the rare earth ions doped glasses for laser applications. The various radiative parameters such as line strengths, optical intensity, and radiative rates from the higher energy levels, including $^5F_4$ + $^5S_2$, $^5F_5$, $^5I_4$, $^5I_5$, $^5I_6$ and $^5I_7$, to the ground state, $^5I_8$ have been reported and discussed. The influence of the Yb^{3+} and Ba$_2$CO$_3$ concentrations on the upconversion and downconversion photoluminescence emission intensities of the glasses prepared have been investigated by pumping with 450 nm and 976 nm excitation sources. Under 450 nm and 976 nm, the NIR photoluminescence emissions reveal a band ranging from 980 nm to 1220 nm attributing to an overlap between Yb^{3+} and Ho^{3+} transitions. The influence of Yb^{3+} concentration on photoluminescence lifetime at the $^2F_{5/2} \rightarrow {}^2F_{7/2}$, $^5F_4$ + $^5S_2$ $\rightarrow ^5I_8$ and $^5I_6 \rightarrow ^5I_8$ transitions under 976 nm laser excitation has been studied and reported. The results indicate that lifetime decreases with increasing Yb^{3+} concentration attributing to an efficient energy transfer from Yb^{3+} to Ho^{3+} ions. The energy transfer efficiency from Yb$^{3+} \rightarrow$ Ho^{3+} has been examined, which rises from 30% to 47% upon increasing Yb^{3+} content. Nevertheless, it decreases with the mixing of BaF$_2$ and Ba$_2$CO$_3$ lattice modifier contents. The results demonstrated that the 1200 nm ($^5I_6 \rightarrow ^5I_8$ transition) has remarkable potential for developing fiber lasers.

Keywords: Barium fluorotellurite glass, Ho, Yb, Judd-Ofelt analysis, OH- groups, photoluminescence, lifetime.

1. Introduction

Trivalent rare-earth (RE^{3+}) ions doped glasses and ceramics have received significant attention over the years from visible to near-infrared (NIR) and mid-infrared for numerous applications, including colour displays, a growing field in medical devices, high-density optical data storage and reading, upconversion laser and visible display devices and indicators [1-3]. This is due to various well-defined electronic transitions characterised by their (4f^n)6s^2 electronic configuration, with the 4f^n-4f^n sub-shell being partially shielded by the 5s, 5p, and 6s electron orbits. As a consequence, leading to host-induced splitting and emitting several light emissions at different wavelengths upon doping with glasses or ceramics [4]. Among these RE^{3+} ions, holmium (Ho^{3+}) is an attractive, active ion because of its several electronic transitions occurring in the visible spectrum, including $^5F_3 \rightarrow ^5I_8$(blue), $^5S_2 \rightarrow ^5I_8$ (green) and $^5F_3 \rightarrow ^5I_8$ (red) transitions. These transition levels have enormous potential for developing white light luminescence, solid-state lasers, efficient fibre lasers, photothermal therapy, temperature sensors, biological imaging, biological labels, and short-wavelength lasers [5-8]. Besides, the Ho^{3+} ion emits NIR photoluminescence emission at $^5I_6 \rightarrow ^5I_8$ transition corresponding to 1200 nm wavelength. This appeals to the development of optical fibre lasers in the O-band for biological imaging [9,10]. For instance, the $^5I_6 \rightarrow ^5I_8$ transition coincides with the high optical

transparency region of the electromagnetic spectrum, which has the advantages of reduced absorption, scattering, and deep penetration depth for biological tissue imaging.

The currently available 976-980 nm diode lasers cannot be used directly to pump Ho^{3+} ions unless it is codoped with a sensitiser such as Yb^{3+}, Tm^{3+} and Er^{3+} ions, which have strong absorption bands around 800 and 980 nm [11-16]. For example, the $^2F_{7/2} \rightarrow ^2F_{5/2}$ transition of Yb^{3+} matches with the intermediate transitions of Ho^{3+} ions facilitating efficient energy transfer mechanisms from Yb^{3+} ($^2F_{5/2}$) to Ho^{3+} ($^5F_4$, $^5S_2$, and $^5I_6$) transitions [6]. Over the years, various glass host materials such as fluorophosphate, silicate, tellurite, and oxyfluoride have been codoped with Ho^{3+}:Yb^{3+} ions [6-10] to investigate their physical and optical properties for the applications mentioned above. Among these, tellurium oxide-based glasses have been studied extensively. This is due to their remarkable properties in terms of the high solubility of RE^{3+} ions, low melting point and stability against crystallisation, non-hygroscopic nature, high refractive index and transmission window, and low phonon energy [3]. Moreover, incorporating alkali oxides, alkaline earth oxides, transition metal oxides and fluoride lattice modifiers into tellurium oxide-based glass hosts tends to decrease the phonon energy. For instance, adding barium fluoride (BaF$_2$) to tellurium oxide-based glass decreases tellurite glass's phonon energy from 750 cm^{-1} to about 645 cm^{-1} owing to BaF$_2$ low phonon energy of 330 cm^{-1} [17]. Consequently, this reduces the nonradiative and multiphonon relaxation mechanism to promote optical transitions in the RE^{3+} ions and improve the radiative transition probability processes [18].

Most tellurium oxide-based glasses doped or codoped with Ho^{3+} or Ho^{3+}:Yb^{3+} ions focused on the 2 μm wavelength for laser application with limited information on the visible and NIR around 1.2 μm wavelength lasers. Here are some examples of Ho^{3+} and Ho^{3+}: Yb^{3+} doped/codoped glasses and ceramics for upconversion and NIR laser applications reported. Wang et al. [19] fabricated various Ho^{3+}/Yb^{3+} codoped TeO$_2$-BaF$_2$-Yb$_2$O$_3$ glasses by varying BaF$_2$ concentration and investigated the luminescence properties at 1200 nm under 915 nm excitation [19]. They reported increases in the luminescence intensity at 1200 nm with increasing the BaF$_2$ concentration and obtained an optical gain of 1.884 dB/cm for 5 cm long fluorotellurite microstructure fiber. Azam et al. [18] recently synthesised Ho^{3+}/Yb^{3+} doped and codoped TeO$_2$-ZnO, TeO$_2$-ZnO-WO$_3$ and TeO$_2$-ZnO-WO$_3$-TiO$_2$, which were optically characterised by employing the optical absorption and upconversion photoluminescence. It was reported that the upconversion emission intensity at 549 nm, 658 nm, and 754 nm was enhanced about 57 times, 342 times, and 480 times upon codoping with 3 mol% of Yb^{3+} under a 980 nm excitation laser. Similarly, Kamma et al.[20] prepared Ho^{3+} doped lead–germano–tellurite glass and investigated its upconversion emission at room temperature under 532 nm and 762 nm excitation. They observed that the upconversion intensity improved significantly after the glass was heat-treated. Additionally, Neto et al.[21] fabricated Ho^{3+} doped PbGeO$_3$-PbF$_2$-CdF$_2$ transparent glass ceramic. An intense red upconversion emission was detected by exciting with a 980 nm diode laser. Besides all these, Ho^{3+}:LiLuF$_4$ and Ho^{3+}:LaF$_3$ have been studied as active gain media for solid-state lasers emitting in the green emission spectral region [22].

In this report, we synthesised and characterised Ho^{3+}, Yb^{3+}-singly doped and Ho^{3+}: Yb^{3+} codoped barium fluorotellurite glasses by changing Yb^{3+} and lattice modifier to understand the local structural environment and optical properties. The spectroscopic properties, including hydroxyl (OH-) concentration in the mid-infrared and lasing properties such as Judd-Ofelt (JO) intensity parameters (Ω_2, Ω_4 and Ω_6), were evaluated from the UV-visible-NIR absorption spectra. The JO parameters are utilised to determine various radiative parameters such as spontaneous emission or radiative transition probabilities (A_R), radiative lifetimes (τ_R), and photoluminescence branching ratios (β_R). The photoluminescence (PL) emissions and lifetime

2

properties were obtained using 450 nm and 980 nm excitation sources. The energy transfer mechanism between Ho^{3+} and Yb^{3+} was looked into under 450 and 980 nm excitations.

2. Experimental Methods

2.1 Glass preparation

High-purity materials such as TeO_2 (≥99.99%), ZnO (99.99%), BaF_2 (99.99%), Yb_2O_3 (99.99%), and Ho_2O_3 (99.99%) purchasing from Alfa Aesar were utilised to synthesise the based glasses. Melting and quenching techniques were employed to prepare Yb^{3+}, Ho^{3+}-singly doped and Ho^{3+}:Yb^{3+} codoped glasses of nominal composition range in mol%: (80-x-y)TeO_2-10ZnO-10BaF_2-yHo_2O_3 (where y=0, 0.5)-xYb_2O_3 (where, x=0, 0.25, 0.5) [named: HTBZ1(y=0), HYTBZ2 (x=0), HYTBZ3, HYTBZ5] and (80-x-y)TeO_2-10ZnO-10(BaF_2-Ba_2CO_3)-0.5Ho_2O_3-0.25Yb_2O_3 [assigned to HYTBZ4]. About 30g batch of high purity stoichiometric composition was initially weighed with an appropriate amount of each raw material, mixed thoroughly using a mortar and a pestle for about 20 min. The powdered mixture in the mortar was collected into a gold crucible and melted at 750–800 °C for about 3 h using an electrical furnace (Elite Thermal Systems Limited, Market Harborough, UK) under a dry oxygen atmosphere until a homogeneous mixture was obtained. The main purpose of purging with high-purity oxygen gas is to control and minimise moisture and OH-ion content in the glass melt. The molten glass was decanted into a pre-heated brass mould at 300 °C for 3 h and placed in the annealed furnace for about 4h to eradicate thermal strains, stress, and air bubbles. Finally, glass blocks prepared with dimensions of $2 \times 4 \times 1$ cm^3 were obtained and polished for optical and photoluminescence property characterisations.

2.2 Characterisation

The polished glasses' refractive index and density were measured using a Prism Coupler (Metricon model 2010/M) with a 633 nm excitation laser and Thermo Pycnomatic ATC Helium Pycnometer. Mid-infrared optical absorbance spectra were collected using a Vertex 70 FITR spectrometer (Brucker, Coventry, UK) over 8 cm^{-1} resolution between 4000 and 400 cm^{-1} to evaluate the hydroxy (-OH) content in the as-prepared glasses. A Perkin Elmer UV/VIS/NIR Lambda 950 spectrometer of 0.1 nm spectral resolution was employed to record the UV-visible-NIR absorption spectra at room temperature (20 ºC) in the spectral range between 250 nm and 2500 nm. An Edinburgh FS920 spectrometer (Edinburgh Instruments, Livingston, UK) was also utilised to collect photoluminescence emission by exciting with 450 and 976 nm diode laser sources in the wavelength range of 500–800 nm and 900–1500 nm at room temperature. Similarly, the photoluminescence decay curves for the glasses prepared were obtained using an FS920 spectrometer equipped with a 976 nm source at room temperature to determine the lifetime.

3. Results and discussions

3.1. Physical Properties and Hydroxyl (OH) concentration Analysis

The refractive index and density values of Yb^{3+}, Ho^{3+} singly doped and Ho^{3+}-Yb^{3+} codoped barium fluorotellurite glass series fabricated are shown in Table 1. The refractive index increases slightly with increasing Yb^{3+} and replace a portion of BaF_2 content with Ba_2CO_3 concentration. This is attributed to the rising molar and electronic polarisabilities of oxide ions. On the other hand, the density of the glasses remains relatively the same. The hydroxyl (OH^-) groups in tellurite base glasses have a strong absorption from 2500 cm^{-1} to 3500 cm^{-1}, which is attributed to the fundamental stretching vibration. The presence of the OH^- group in a glass network can quench visible and NIR photoluminescence emission intensity and lifetime through phonon-assisted processes and interactions with RE^{3+} ions. The mid-infrared

3

absorption spectra of samples HTBT1, HYTBT2, HYTBT3, HYTBT4 and HYTBT5 [inset pictures shown in Figure 1 were measured using a Brucker Vertex 70 FTIR spectrometer at room temperature. The absorption coefficient (α_{OH}) of the OH$^-$ vibration peak centred at 3000 cm^{-1} was determined for each sample with a thickness of L using the Beer-Lambert law equation [3], which is given by:

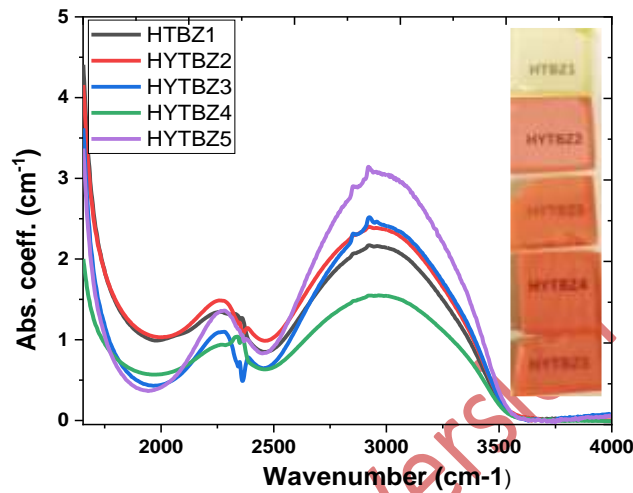$$\alpha_{OH} = \frac{ln\left(\frac{T(\%)}{100}\right)}{L} = \frac{2.303 x A}{L} \tag{1}$$

Figure 1: Infrared absorption spectra of singly Yb^{3+}, Ho^{3+} doped, and Ho^{3+}:Yb^{3+} codoped fluorotellurite glasses and the inset showing photographs of various glasses prepared.

Table 1: OH absorption coefficient, α_{OH} (cm^{-1}), and concentration, N_{OH^-}(ions/cm^{-3}), at mid-infrared wavelengths of 3000 cm^{-1}.

Sample ID	Refractive index	Density(g/cm³)	$\alpha_{OH}(cm^{-1})$	OH- conc. (ppm)
HTBZ1	1.987	5.623	2.16	**43.9**
HYTBZ2	2.007	5.675	2.37	**48.9**
HYTBZ3	2.013	5.618	2.44	**49.8**
HYTBZ4	2.162	5.650	1.54	**30.9**
HYTBZ5	2.029	5.663	3.09	**62.8**

The OH$^-$ content, $N_{OH^-}(ppm)$, in the glass was estimated from equation (2) by using the OH$^-$ absorption coefficient obtained from the equation (1). The results were converted into part per million (ppm) [3,23].

$$N_{OH^-} = \frac{N_{AVO}}{\varepsilon}\alpha_{OH} \tag{2}$$

where L is the glass thickness (cm), A is the absorbance, ε is the OH$^-$ group molar absorptivity in the tellurite glass (4.91 × 10^4 cm^{2}mol^{-1}) [23], and N_{AVO} represents Avogadro's constant (6.02 × 10^{23} mol^{-1}). Figure 1 shows that the absorption coefficient of the OH$^-$ vibration band occurring at 3000 cm^{-1} for sample HTBZ1 is lower than the remaining glass samples. Nonetheless, the rest of the glass samples codoping with Ho^{3+}:Yb^{3+} increase in absorption coefficient by increasing Yb^{3+} content leading to a surge in OH- concentration, as shown in Table 1. On the other hand, sample HYTBZ4 exhibits a very low OH concentration compared to the other glasses.

4

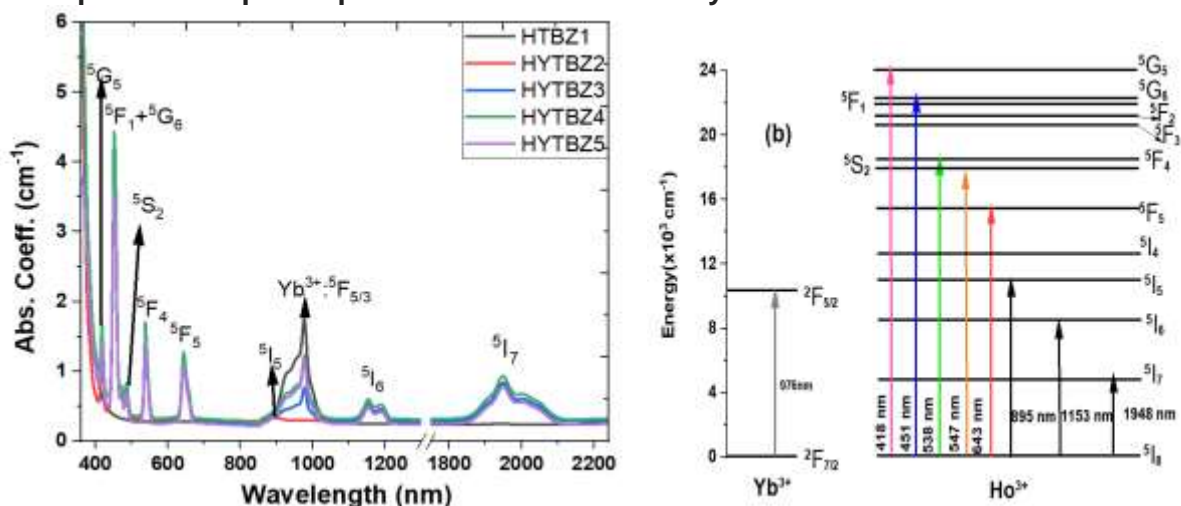## 3.2. Optical absorption spectra and Judd-Ofelt analysis

Fig. 2: (a) UV-visible-NIR absorption coefficient spectra of Yb^{3+}, Ho^{3+} single doped and Ho^{3+}-Yb^{3+} codoped barium fluorotellurite glass series, (b) Partial energy level diagram of Ho^{3+} ion.

As-prepared glasses' absorbance spectra ranged from 250 nm to 2500 nm were measured using a UV-visible-NIR spectrophotometer, which was converted to absorption coefficient using equation(1). The absorption peaks centred at 418, 451, 487, 538, 643, 952, 976, 1153 and 1948 nm are attributed to 4f-4f intra manifold transitions of Ho^{3+} ion and Yb^{3+} ion from the ground state to the various excited states as illustrated in Fig 2(b). The Ho^{3+} ions peaks correspond to transitions from the ground state to distinctive excited states, namely $^5I_8 \rightarrow {}^5G_5$, $^5F_1 \& {}^5G_6$, $^5S_2$, $^5F_4$, $^5F_5$, $^5I_5$, $^5I_6$, $^5I_7$ and $^2F_{7/2} \rightarrow {}^2F_{5/2}$ for Yb^{3+} ion, respectively. The crystal field surrounding each of these RE^{3+} ions is inhomogeneous because of the distinguishability of the absorption transitions retained by the Ho^{3+} and Yb^{3+} ions and site-to-site disparities in the crystal field strengths [18, 24].

The Judd-Ofelt (JO) intensity parameters that signify interactions between the Ho^{3+} ions and the fluorotellurite host material crystalline field were calculated using the UV-visible-NIR absorption coefficient shown in Fig. 1 (a). The JO method has been extensively used to study the radiative and non-radiative rates of RE^{3+} ions doped with different host materials for laser application. An integral absorption coefficient ($\int \alpha(\lambda)d\lambda$) of each absorption band comprises of electric dipole ($S_{ed(mes)}(J \rightarrow J')$) and the magnetic dipole ($S_{md}(J \rightarrow J')$) line strength contributions. Henceforth, the measured experimental $S_{ed(mes)}(J \rightarrow J')$ line strengths from the initial transition, J, to the upper energy levels , J', were obtained using the following expression [25- 29];

$$S_{ed(mes)}(J \rightarrow J') = n\left[\frac{3}{n^2+2}\right]^2 \left[\frac{3ch(2J+1)}{8\pi^3 e^2 N_{Ho}} \frac{1}{\bar{\lambda}} \int \alpha(\lambda)d\lambda - \left[\frac{(n^2+2)^2}{9n}\right]n^3 S_{md}(J \rightarrow J')\right] \qquad \textbf{(3)}$$

where **c** is the velocity of light, **h** is the Planck's constant, **e** is the charged electron, n is the refractive index, $\bar{\lambda}$ is the average absorption peak wavelength for the transition under consideration, N_{Ho} being the concentration of Ho^{3+} ions, and **2J+1** is the degeneration of the initial (emitting) state delineated.

The magnetic dipole $S_{md}(J \rightarrow J')$ transition contribution of the line strength is given by an expression [25,26, 29].

$$S_{md}(J \rightarrow J') = \mu_B^2 |[|< J||L + 2S||J' >|]|^2 \qquad (4)$$

5

where **μ$_B$= (ℏ/2mc)** and the magnetic dipole matrix elements are located in the bracket terms, orbital **L** and spin **S** angular momenta even-parity tensors. The transitions between different energy levels must conform to the selection rules as $\Delta S = \Delta L = 0$ and $\Delta J = 0, \pm 1$ for a magnetic dipole line strength to exist. Based on the selection rule, the only transition with magnetic line strength contribution is ${}^5I_8 \rightarrow {}^5I_7$, which was subtracted from the experimental result to obtain $S_{ed(mes)}$.

Thus, the JO parameters, (Ω_t), are calculated from the electric-dipole transition line strengths by using the expression shown below [26,27, 30]:

$$S_{ed(cal)}(J \rightarrow J') = \sum_{t=2,4,6} \left| |< J||U^{(t)}||J' >| \right|^2 \tag{5}$$

Where $U^{(t)}$ is the squared doubly reduced matrix of the unit tensor operator of the rank t = 2, 4, 6. The eight absorption peaks from Figure 2 (a) were employed to determine the JO parameters via the least square fit method. As shown in Table 2, the magnitude of JO intensity parameters of as-prepared glasses follows the same trend as $\Omega_4 > \Omega_2 > \Omega_6$ for samples HYTBZ2, HYTBZ3, HYTBZ4 and HYTBZ4. The Ω_2 parameter describes asymmetry and covalency. Thus, the Ω_2 parameter increases from samples HYTBZ2 to HYTBZ4 by codoping with Yb^{3+} ions and substituting a portion of BaF$_2$ with Ba$_2$CO$_3$ content suggesting structural changes. Besides, the visible to near-infrared absorption peaks are hypersensitivity to covalency parameters, increasing the ligand surrounding the RE^{3+} ions. Similarly, the Ω_4 intensity parameter rises with the additive of Yb^{3+} concentration can be ascribed to an increase in viscosity due to the highly polarised surrounding Ho^{3+} [31, 32]. Furthermore, the Ω_6 parameter increases with the addition of Yb^{3+} and Ba$_2$CO$_3$ into the glass composition, indicating a decrease in the Ho^{3+}-O covalency and fraction of non-bridge oxygen ions [33,34]. Likewise, as the concentration of the Yb^{3+} ions increased the JO intensity parameters of sample HYTBZ5 diminished with the same trend as $\Omega_4 > \Omega_2 > \Omega_6$, which correlates with Ho^{3+} doped lead tungsten tellurite glasses reported elsewhere [33]. The difference in the JO parameters for as-prepared glasses is ascribed to structural transformation. However, substituting a low concentration of Ba$_2$CO$_3$ in exchange for BaF$_2$ (HYTBZ4) resulted in sizeable structural modification and rearrangement in the glass network owing to increased JO parameters, as shown in Table 2.

Furthermore, the spectroscopic quality factor (Ω_4/Ω_6) is an important parameter to predict stimulated emission and intensity of lasing in the gain medium. The Ω_4/Ω_6 factor of Ho^{3+} singly doped fluorotellurite glass is greater than those glass samples fabricated by codoping with Ho^{3+}: Yb^{3+}. On the other hand, the Ω_4/Ω_6 factor for Ho^{3+}: Yb^{3+} ions doped fluorotellurite glasses decreases with increasing Yb^{3+} ions content but increases slightly with mixing BaF$_2$ with Ba$_2$CO$_3$ contents.

Table 2: Judd-Ofelt parameters $(\Omega_\lambda \times 10^{-20} cm^2)$ of Ho^{3+} ions in fluorotellurite glasses compared with other fluoride glasses

Sample ID	Ω_2	Ω_4	Ω_6	$\sum \Omega_t$	Ω_4/Ω_6	Trend	Ref
HYTBZ2	3.562	4.666	2.260	10.488	2.26	$\Omega_4 > \Omega_2 > \Omega_6$	Present work
HYTBZ3	3.787	4.343	2.902	11.032	1.49	$\Omega_4 > \Omega_2 > \Omega_6$	Present work
HYTBZ4	3.906	5.034	3.052	11.992	1.65	$\Omega_4 > \Omega_2 > \Omega_6$	Present work
HYTBZ5	3.393	3.850	2.503	9.746	1.54	$\Omega_4 > \Omega_2 > \Omega_6$	Present work

6

The calculated JO parameters obtained from equation (3) shown in Table 2 were used to predict $S_{ed(cal)}$ values via the multiple regression, which are in close approximation to the measured values. The calculated and measured electric dipole line strengths with small RMS values of Ho[3+] and Ho[3+]:Yb[3+] doped fluorotellurite glasses for various ground state absorption bands are illustrated in Table 3. The variation in trends of the measured and calculated electric dipole line strengths are comparable to JO parameters for increasing Yb[3+] ions concentration and substituting a portion of BaF_2 with Ba_2CO_3 content. Some of the inter manifold 4f-4f absorption bands and spectral intensities of the RE[3+] ions are sensitive to their environment, which is characterised by higher values of electric dipole line strengths. Such hypersensitive transitions of RE[3+] ions must satisfy the selection rules $\Delta J \leq 2$, $\Delta L \leq 2$ and $\Delta S = 0$ [27]. For instance, $^5I_8 \rightarrow {}^5F_1 + {}^5G_5$ and $^5I_8 \rightarrow {}^5I_7$ transitions are hypersensitive transitions due to significant variation in the electric dipole line strength values upon increasing Yb[3+] concentration or replacing a portion of BaF_2 content with Ba_2CO_3.

Table 3: Experimental ($S_{ed(mes)} \times 10^{-20}$) and calculated ($S_{ed(cal)} \times 10^{-20}$) line strengths and δ_{rms} deviation of Ho ions in fluorotellurite glass systems

The transition from $^5I_8 \rightarrow$	HYTBZ2		HYTBZ3		HYTBZ4		HYTBZ5	
	$S_{ed(mes)}$	$S_{ed(cal)}$	$S_{ed(mes)}$	$S_{ed(cal)}$	$S_{ed(mes)}$	$S_{ed(cal)}$	$S_{ed(mes)}$	$S_{ed(cal)}$
$^5G_5$	2.019	1.994	2.067	2.227	2.825	2.869	2.912	2.962
$^5F_1 + {}^5G_5$	9.626	9.607	8.953	8.910	10.571	12.647	8.724	8.455
$^5S_2$	0.558	0.541	0.626	0.626	0.736	0.738	0.550	5.794
$^5F_4$	2.105	2.194	2.178	2.209	2.457	2.358	2.212	2.128
$^5F_5$	3.229	3.147	3.029	3.101	3.798	3.793	2.722	2.709
$^5I_5$	1.838	1.927	2.016	2.068	2.695	2.724	2.354	2.231
$^5I_6$	2.232	2.393	2.725	2.793	2.631	2.939	2.062	2.169
$^5I_7$	5.100	5.019	4.941	4.895	5.590	5.728	4.569	4.693
δ_{rms}	1.06×10^{-21}		0.93×10^{-21}		2.05×10^{-21}		0.94×10^{-20}	

Moreover, the JO parameters obtained from the above were utilised to analyse other important parameters such as radiative or spontaneous transition probabilities of emission, branch ratios, and radiative lifetime. The radiative transition probability ($A_r(J \rightarrow J')$) of different energy transitions (between J and J') associating with the electric $S_{ed(cal)}$ and magnetic S_{md} line strength can be expressed as [26- 28].

$$A_r(J \rightarrow J') = \frac{1}{4\pi\varepsilon_0} \frac{64\pi^4 v^3}{3hc^3(2J+1)} \left[n\left[\frac{n^2+2}{3}\right]^2 S_{ed(cal)}(J \rightarrow J') - n^3 S_{md}(J \rightarrow J') \right] \quad (6)$$

The total radiative transition probability (A_T) is defined as the sum of all excited transitions, which is represented as follows.

$$A_T = \sum A_r(J \rightarrow J') \quad (7)$$

The excited state radiative lifetime, τ_R, and theoretical branch ratio, β_R, are calculated from the total radiative transition probability as:

$$\tau_R(J) = [A_T(J)]^{-1} \quad (8)$$

$$\beta_R(J,J') = \frac{A_r(J \rightarrow J')}{\sum A_r(J \rightarrow J')} \quad (9)$$

7

The radiative spectroscopic parameters such as radiative transition probabilities, branching ratios, and radiative lifetime were further determined by employing equations (3) to (6) for all relevant energy transitions of the Ho^{3+} ions, which are summarised in Table 4. The transitions with high values of radiative transition probabilities and branching ratios represent more probability of radiative transition from the excited states to lower energy levels.

Table 4: Predicted spontaneous emission probabilities, total transition probability (A_T), radiative lifetime (τ_R) and the branching ratio of the possible transition levels in the Ho^{3+}/Ho^{3+}:Yb^{3+} doped HYTBZ glass series.

Transition	Wavenumber (cm^{-1})	HYTBZ2		HYTBZ3		HYTBZ4		HYTBZ5	
		A_r(1/s)	β(%)	A_r(1/s)	β(%)	A_r(1/s)	β(%)	A_r(1/s)	β(%)
$^5F_4 + ^5S_2 \rightarrow ^5F_5$	2844	0.5	0.03	0.5	0.02	0.5	0.01	4.0	0.14
$^5F_4 + ^5S_2 \rightarrow ^5I_5$	5260	45.3	3.2	55.4	3.0	59.1	1.8	48.0	1.7
$^5F_4 + ^5S_2 \rightarrow ^5I_5$	7122	31.9	2.2	40.0	2.2	51.7	1.6	42.3	1.6
$^5F_4 + ^5S_2 \rightarrow ^5I_6$	9719	117.1	8.2	141.3	7.7	218.5	6.6	176.7	6.5
$^5F_4 + ^5S_2 \rightarrow ^5I_7$	13277	538.2	37.7	691.1	37.8	1211.0	36.4	993.0	36.4
$^5F_4 + ^5S_2 \rightarrow ^5I_8$	18396	700.0	48.8	899.1	49.2	1785.8	53.6	1463.7	53.6
		$A_T = 1432.5$s^{-1} $\tau_R = 0.698\ ms$		$A_T = 1826.9$ s^{-1} $\tau_R = 0.547\ ms$		$A_T = 3326.7$s^{-1} $\tau_R = 0.301\ ms$		$A_T = 2727.8$s^{-1} $\tau_R = 0.366\ ms$	
$^5F_5 \rightarrow ^5I_5$	4278	1.4	0.4	1.6	0.4	1.8	0.4	1.4	0.4
$^5F_5 \rightarrow ^5I_6$	6872	16.1	4.5	18.7	4.8	20.2	4.7	16.3	4.8
$^5F_5 \rightarrow ^5I_7$	10432	72.9	20.2	77.8	20.1	86.1	20.1	68.2	20.1
$^5F_5 \rightarrow ^5I_8$	15552	270.5	74.9	289.2	74.6	320.6	74.8	253.1	74.6
		$A_T = 360.8$ s^{-1} $\tau_R(J) = 2.77\ ms$		$A_T = 387.4$ s^{-1} $\tau_R(J) = 2.58\ ms$		$A_T = 428.7$ s^{-1} $\tau_R(J) = 2.33\ ms$		$A_T = 338.9$ s^{-1} $\tau_R(J) = 2.95\ ms$	
$^5I_5 \rightarrow ^5I_6$	2597	11.3	5.2	12.9	4.8	13.9	4.9	11.2	4.8
$^5I_5 \rightarrow ^5I_7$	6155	123.0	57.1	155.6	58.2	164.3	57.9	134.4	58.2
$^5I_5 \rightarrow ^5I_8$	11274	81.0	37.6	98.9	37.0	105.2	37.2	85.4	37.0
		$A_T = 215.3$ s^{-1} $\tau_R(J) = 4.6\ ms$		$A_T = 267.4$ s^{-1} $\tau_R(J) = 3.74\ ms$		$A_T = 283.4$ s^{-1} $_R(J) = 3.53\ ms$		$A_T = 231.1$ s^{-1} $\tau_R(J) = 4.32ms$	
$^5I_6 \rightarrow ^5I_7$	3558	41.2	14.0	46.7	12.9	40.7	13.0	40.6	13.0
$^5I_6 \rightarrow ^5I_8$	8677	253.7	86.0	315.6	87.1	273.0	87.0	273.0	87.0
		$A_T = 294.9$ s^{-1} $\tau_R(J) = 3.39\ ms$		$A_T = 362.4$ s^{-1} $\tau_R(J) = 2.76\ ms$		$A_T = 313.7$ s^{-1} $\tau_R(J) = 3.19\ ms$		$A_T = 313.7$ s^{-1} $\tau_R(J) = 3.19\ ms$	
$^5I_7 \rightarrow ^5I_8$	5119	125.2	100	182.2	100	191.8	100	162.1	100
		$A_T = 125.2\ s^{-1}$ $\tau_R(J) = 7.98\ ms$		$A_T = 182.2\ s^{-1}$ $\tau_R(J) = 5.49\ ms$		$A_T = 191.8\ s^{-1}$ $\tau_R(J) = 5.21\ ms$		$A_T = 162.1\ s^{-1}$ $\tau_R(J) = 6.17\ ms$	

For example, the $^5F_4 + {}^5S_2 \rightarrow {}^5I_8$ transition (~545 nm) has the most significant values of radiative transition probabilities, and branching ratios in all the samples synthesised ranging from 700.05 s^{-1} to 1785.8s^{-1} for (A_T) and 48.8 to 53.6 % for **β.** This indicates that most of the photons in the $^5F_4 + {}^5S_2$ states would radiate into the $^5I_8$ ground state transition. Thus, such high radiative parameters validate and agree with the strong green photoluminescence intensity observed experimentally under 450 nm and 976 nm excitations. Similarly, higher radiative transition probabilities and branching ratios were obtained from the $^5F_5 \rightarrow {}^5I_8$ (650 nm) $^5F_4 + {}^5S_2 \rightarrow {}^5I_7$ (750) transition, as listed in Table 4. In addition, the radiative transition probabilities or rates from $^5I_6 \rightarrow {}^5I_8$ transition predicted by JO theory range from 253.7 to 315.6 S^{-1} leading to longer radiative lifetimes with an average branching ratio of ~86%. This result corroborates with the intense NIR photoluminescence emission observed experimentally at 1159 nm transition.

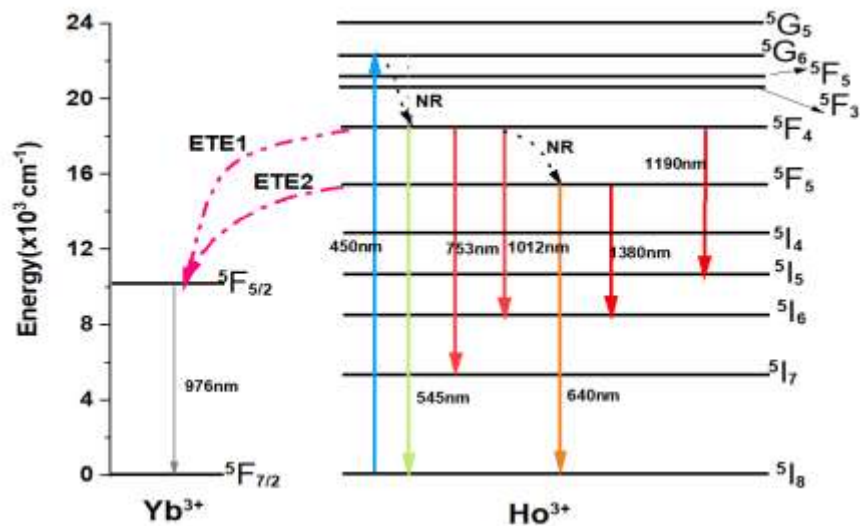### 3.3. Photoluminescence emissions and energy transfer under 450 nm and 980 nm excitations

Fig.4: Partial energy level diagrams for Ho^{3+} and Ho^{3+}:Yb^{3+} visible and NIR photoluminescence emission observed under 450 nm excitation.
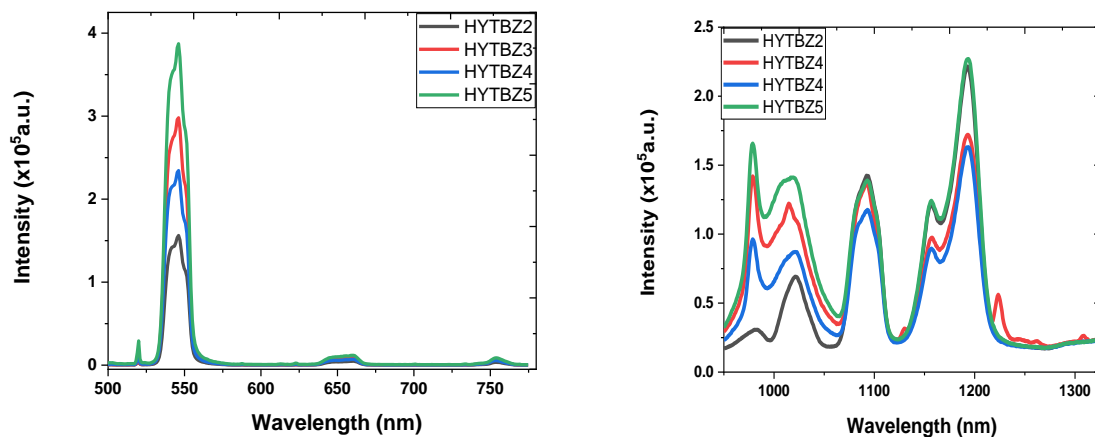

Fig. 5: Downconversion photoluminescence emission of Ho^{3+} and Ho^{3+}:Yb^{3+} doped fluorotellurite glasses under 450 nm excitation (a) visible and (b) NIR wavelength ranges.

9

Figure 4 illustrates a partial energy diagram for Ho^{3+} and Yb^{3+} ions under a 450 nm excitation source to measure visible to NIR photoluminescence emissions. The Ho^{3+} ion is initially excited with 450 nm from the ground state, $^5I_8$, to the excited state, $^6G_5$, through the ground state absorption process. These electrons in the $^6G_5$ level undergo non-radiative decay to the $^5F_4$ energy level via a multi-phonon relaxation process. This is followed by radiative relaxation to $^5I_8$ transition, leading to the intense green emission at 545 nm, shown in Figure 5 (a). The electrons in the $^5F_4$ state further depopulate through the multi-phonon relaxation process to the $^5F_5$ state, which relaxes radiatively to the ground state $^5I_8$ emitting weak red emission at 640 nm. It is vital to mention that the photoluminescence emission at 545 nm is less intense for Ho^{3+} singly doped fluorotellurite glass. However, codoping with Yb^{3+} and substituting a portion of BaF_2 content with Ba_2CO3 lead to increased photoluminescence emission intensity. Besides, the NIR photoluminescence emissions centred at 1156 and 1192 nm match the $^5F_4 \rightarrow ^5I_5$ transition, as depicted in Figure 5(b). In contrast, the photons absorbed by the Ho^{3+} ions under 450 nm excitation can further be transferred to Yb^{3+} from either $^5F_4 \rightarrow ^2F_{5/2}$ or $^5I_5 \rightarrow ^2F_{5/2}$ through the energy transfer process and phonon-assisted ET1 and ET2. This emits intense overlap photoluminescence emission range from 950 to 1070 nm for Ho^{3+} and Yb^{3+} as illustrated in Figure 4, ascribing to $^5F_4 \rightarrow ^5I_6$ and $^2F_{5/2} \rightarrow ^2F_{7/2}$ transitions.

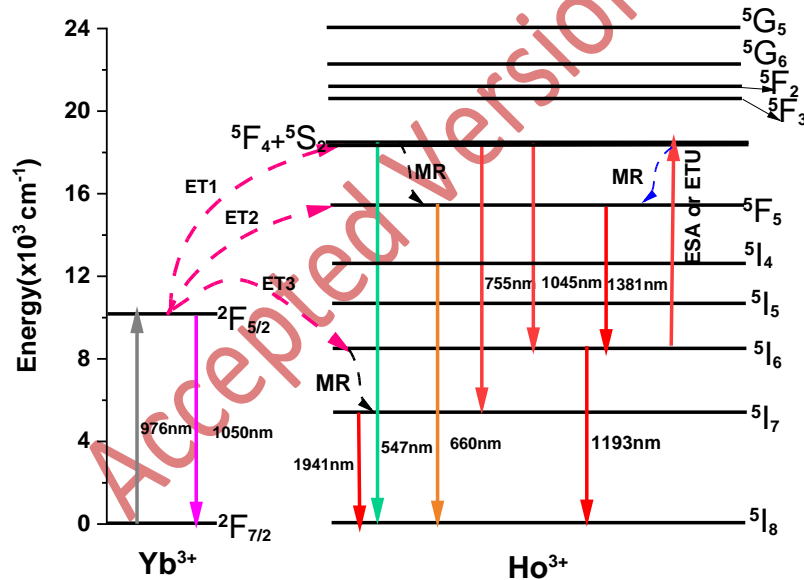

Fig.6: Partial energy level diagrams for Ho^{3+} and $Ho^{3+}:Yb^{3+}$ visible and NIR photoluminescence emission observed under 976 nm excitation.

The visible and NIR photoluminescence emission properties of Ho^{3+} singly doped and $Ho^{3+}:Yb^{3+}$ codoped fluorotellurite glasses were investigated under a 976 nm diode laser excitation wavelength, as shown in Figure 6. Ho^{3+} ions in singly-doped glass do not absorb at 976 nm by themselves. Therefore, no emission is observed experimentally from visible to NIR. Moreover, upon exciting the $Ho^{3+}:Yb^{3+}$ codoped glass samples with a 976 nm pumping scheme, the ground state of Yb^{3+} ($^2F_{7/2}$) is absorbed to populate the excited state of Yb^{3+} ($^2F_{5/2}$) via the ground state absorption process. Most of the photons in the Yb^{3+} ($^2F_{5/2}$) excited state can be de-excited radiatively, leading to a NIR emission peak at 1050 nm. This corresponds to the $^2F_{5/2} \rightarrow ^2F_{7/2}$ transition. Additionally, some of the photons in the Yb^{3+} ($^2F_{5/2}$) excited state can be transferred utilising the phonon-assisted energy transfer process to the neighbouring

Ho^{3+} through three main routes ET$_1$ (Yb^{3+}:^{2}F$_{5/2}$ → Ho^{3+}:^{5}F$_4$ + ^{5}S$_2$), ET$_2$(Yb^{3+}:^{2}F$_{5/2}$ → Ho^{3+}:^{5}F$_5$), and ET$_3$ (Yb^{3+}:^{2}F$_{5/2}$ → Ho^{3+}:^{5}I$_6$), respectively.
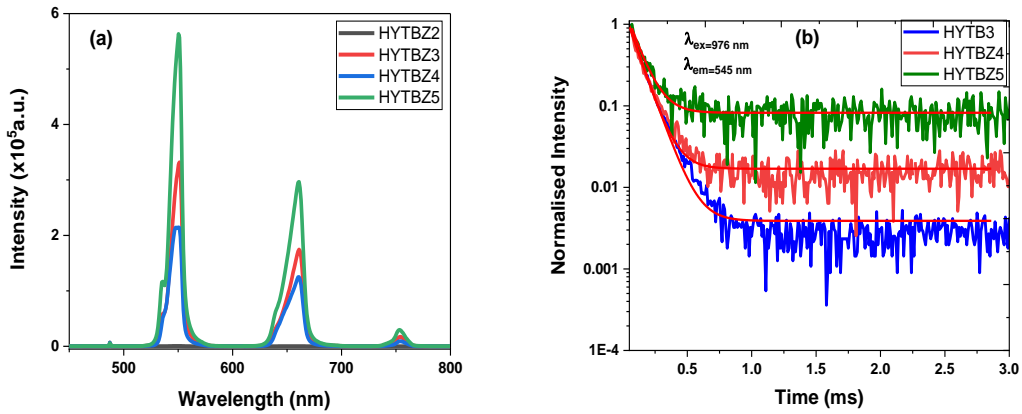

Fig 7: (a) Upconversion photoluminescence emission spectra of Ho doped and Ho^{3+}: Yb^{3+}-codoped glasses under 978 nm excitation source, (b) photoluminescence–decay curves at 545 nm.

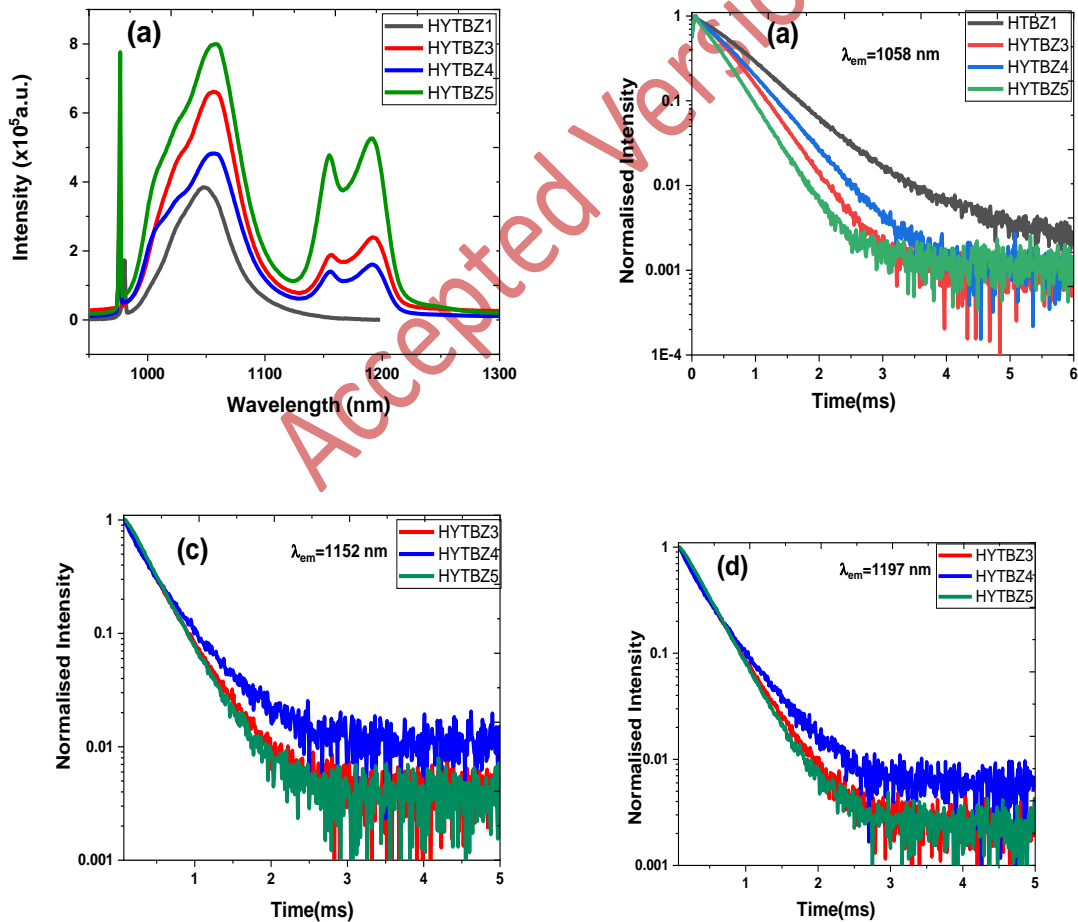
Fig. 8: (a) Near-infrared photoluminescence emission spectra of Ho-doped and Ho^{3+}: Yb^{3+}-codoped glasses under 978 nm excitation source: (**b**)-(**d**) photoluminescence–decay curves Ho^{3+} at ^{5}F$_4$ and ^{5}I$_6$ transitions.

11

The photons transfer through ET_1 (Ho^{3+}:$^5F_4 + ^5S_2$) path by excited state absorption or energy transfer process from Yb^{3+}:$^2F_{5/2}$ state undergo radiative decay to emit Ho^{3+}:$^5F_4 + ^5S_2 \rightarrow {}^5I_8$ and Ho^{3+}:$^5I_7 \rightarrow {}^5I_8$ leading to the intense upconversion emissions at 552 nm and 755 nm, as shown in Figure 7(a). Likewise, part of the photons in the Ho^{3+}:$^5F_4 + ^5S_2$ state can undergo non-radiative decay by multi-phonon relaxation to Ho^{3+}:$^5F_5$ or ET_2(Yb^{3+}:$^2F_{5/2} \rightarrow$ Ho^{3+}:$^5F_5$) energy transfer process can occur and then decay radiatively to the ground state Ho^{3+}:$^5I_8$ emitting 660 nm upconversion. On the other hand, energy transfer processes occur via ET_1 (Yb^{3+}:$^2F_{5/2} \rightarrow$ Ho^{3+}:$^5F_4 + ^5S_2$), and ET_3 (Yb^{3+}:$^2F_{5/2} \rightarrow$ Ho^{3+}:$^5I_6$) can generate NIR emissions at 1050 nm and 1196 nm matching with $^5F_4 + ^5S_2 \rightarrow {}^5I_6$, and $^5I_6 \rightarrow {}^5I_8$ transitions depicted in Figure 8(a), respectively. Alternatively, part of the Ho^{3+}:$^5I_6$ ions can further populate to the higher energy levels such as Ho^{3+}:$^5F_4 + ^5S_2$ state through excited-state absorption or energy transfer upconversion process (ETU) to generate the upconversion emission shown in Figure 6.

3.4. Yb^{3+} , Ba$_2$CO$_3$ modifier, and OH- effect on the Yb^{3+} :$^2F_{5/2}$, Ho^{3+}: $^5F_4 + ^5S_2$ and Ho^{3+}: $^5I_6$ transitions lifetime.

The upconversion and downconversion photoluminescence decay curves for all the fabricated samples were analysed to determine the energy transfer efficiency mechanism. Many studies have suggested that the lifetime of the rare earth ions transitions depends on the glass system's phonon energy. This relates to the base glass composition network former and added lattice modifier network [35- 37]. Besides, it is well established that the existence of the OH$^-$ group in the glass host can significantly promote the non-radiative process resulting in lifetime quenching. Therefore, the photoluminescence decay lifetimes of singly Yb^{3+} and Ho^{3+}:Yb^{3+}doped glasses were measured for Yb^{3+}:$^2F_{5/2}$, Ho^{3+}:$^5F_4 + ^5S_2$ and Ho^{3+}: $^5I_6$ transitions by exciting the samples with 976 nm excitation source at room temperature. Figures 7(b) and 8(b-d) show photoluminescence decay curves for singly doped Yb^{3+} and codoped Ho^{3+}:Yb^{3+} at Yb^{3+}:$^2F_{5/2}$ and Ho^{3+}: $^5I_6$ transitions, which were fitted with single exponential function to determine the measured lifetime. The measured lifetime obtained from various samples and transitions is summarised in Table 5 below. The lifetime of the Ho^{3+} at $^5F_4 + ^5S_2$ transitions increases slightly with increasing Yb^{3+} and doping with BaF$_2$ and Ba$_2$CO$_3$ contents. However, the Yb^{3+}:$^2F_{5/2}$ transition decreases with increasing Yb^{3+} concentration. This is attributed to highly energy transfer efficiency, as shown by a significant reduction in the Yb^{3+} lifetime in the Yb^{3+}-Ho^{3+} glasses in contrast to the Yb^{3+} singly-doped glass. The lifetime of sample HYTBZ4 rises by 11% over sample HYTBZ3 at Yb^{3+}:$^2F_{5/2}$ and Ho^{3+}:$^5I_6$ transitions ascribing to the inadequacy in energy transfer efficiency and difference in OH ion concentration discussed in Table 1.

Table 5: Measure lifetime obtained from Yb^{3+} and Ho^{3+}: transitions and energy transfer efficiency.

Sample ID	$\tau_m(ms)$				$\eta_{ET(Yb \rightarrow Ho)}$	$W_{MP}(s^{-1})$ $^5F_4 + ^5S_2 \rightarrow {}^5I_8$	$W_{MP}(s^{-1})$ $^5I_6 \rightarrow {}^5I_8$
	Ho^{3+}:$^5F_4 + ^5S_2$	Yb^{3+}:$^2F_{5/2}$,	Ho^{3+}: $^5I_6$ (1152nm)	Ho^{3+}: $^5I_6$ (1196nm)			
HTBZ1	-	0.769	-	-			
HYTBZ2	-	-	-	-			
HYTBZ3	0.094	0.538	0.352	0.365	0.30	9837.9	2509.7
HYTBZ4	0.113	0.596	0.377	0.373	0.23	7057.8	1857.8
HYTBZ5	0.131	0.410	0.347	0.366	0.47	6145.1	2522.0

The photoluminescence lifetime measured was employed to determine whether the Yb^{3+} ion is a suitable sensitiser for the Ho^{3+}:Yb^{3+} codoped fluorotellurite glasses fabricated by determining energy transfer efficiency ($\eta_{ET(Yb \rightarrow Ho)}$) from Yb^{3+} ions to Ho^{3+} ions. The energy

transfer efficiency between Yb^{3+} ions and Ho^{3+} ions was evaluated by the following equation [37]:

$$\eta_{ET(Yb \to Ho)} = 1 - \frac{\tau_{Yb(Ho)}}{\tau_{Yb}} \qquad (10)$$

where $\tau_{Yb(Ho)}$ is the lifetime at Yb^{3+} :^{2}F$_{5/2}$ transition in the Ho^{3+}:Yb^{3+} ions codoped glasses and τ_{Yb} being a singly doped glass with Yb^{3+}, respectively. It is observed that the energy transfer efficiency increases with Yb^{3+} concentration, as illustrated in Table 4.

Furthermore, the multiphonon de-excitation rate, W_{MP}, component of the non-radiative decay rate contribution for depopulation of the metastable state from Ho^{3+}: ^{5}F$_4$ + ^{5}S$_2$ and ^{5}I$_6$ transitions to the ground state Ho^{3+}: ^{5}I$_8$ were calculated by [25,37] :

$$W_{MP} = \tau_m^{-1} - \tau_r^{-1} - W_{OH} \qquad (11)$$

where τ_m^{-1} and τ_r^{-1} are the measured radiative rate and estimated radiative decay rates obtained from JO analysis of the Ho^{3+}:^{5}F$_4$ + ^{5}S$_2$ and Ho^{3+}: ^{5}I$_6$. W_{OH} is the energy transfer rate between Ho^{3+} and the OH$^-$. According to Dai et al. [36], the energy transfer rate between Ho^{3+} and the OH$^-$ groups can be expressed:

$$W_{OH} = 8\pi C_{Ho,Ho} N_{Ho} N_q \qquad (12)$$

where N_{Ho} is the Ho^{3+} concentration (acceptor concentration) and N_q is the density of the quenching site, which is proportional to OH- concentration [$N_q = \chi N_{OH}$, χ is the empirical factor, which is about χ=15% for the modified tellurite glass], and $C_{Ho,Ho}$ is the microparameter of the transfer process. The value of $C_{Ho,Ho}$ for modified tellurite glass can be estimated based on the Forster-Dexter theory as follows [37]:

$$C_{Ho,Ho} = \frac{3cA_r(2J+1)}{8\pi^4 n^2 (2J'+1)} \int \sigma_{ems}^D(\lambda) \, \sigma_{abs}^A(\lambda) d\lambda \qquad (13)$$

where $\sigma_{ems}^D(\lambda)$ and $\sigma_{abs}^A(\lambda)$ donor-acceptor energy transfer overlap between the emission and absorption bands of the donor and acceptor. Table 4 shows the W_{MP} for Ho^{3+}: ^{5}F$_4$ + ^{5}S$_2$ → ^{5}I$_8$ and ^{5}I$_6$→^{5}I$_8$ transitions increases with increasing Yb^{3+} concentration. Nevertheless, the mixing addition of BaF$_2$ and Ba$_2$CO$_3$ leads to a significant decrease in the multiphonon relaxation rate, which could be attributed to the variation in the host material and its local field symmetry surrounding the rare earth ion site [38]. Furthermore, the significant increase in multiphonon relaxation rate of Ho^{3+}: ^{5}F$_4$ + ^{5}S$_2$ → ^{5}I$_8$ and ^{5}I$_6$→^{5}I$_8$ transitions could boost the 976 nm pumping efficiency in the Ho^{3+}:Yb^3 codoped glass series.

4. Conclusions

Series of Yb^{3+} singly, Ho^{3+} singly, and Ho^{3+}:Yb^{3+} doped/codoped barium fluorotellurite glasses have been prepared and characterised by optical absorption, photoluminescence, and decay studies. The intensity parameters and radiative properties of the dominant transition energy levels of the Ho^{3+} ion have been investigated using the JO theory. The JO parameters obtained from the Ho^{3+} singly doped and Ho^{3+}:Yb^{3+} codoped glasses follow the trend $\Omega_4 > \Omega_2 > \Omega_6$. The change in the Ω_2 with Yb^{3+} and Ba$_2$CO$_3$ contents is ascribed to variation in the asymmetry of the ligand field around the rare earth ion site and the degree of covalency of the Ho-O bond. While $\Omega_4 \text{ and } \Omega_6$ values are related to viscosity and stiffness of the host glass, which decreases with Yb^{3+} content. The effect of Yb^{3+} and Ba$_2$CO$_3$ contents on the upconversion and NIR downconversion photoluminescence emission of the Yb^{3+} singly doped and Ho^{3+}:Yb^{3+} codoped glasses have been studied. The upconversion, NIR emission intensity, and lifetime centred at 550, 661, 742, and 1196 nm increase significantly with Yb^{3+} concentration, which is accredited to an efficient energy transfer from Yb^{3+} → Ho^{3+};

13

nonetheless decreases with substitution of a small fraction of BaF_2 with Ba_2CO_3 content. Even though the OH- ions concentration increases remarkably with Yb^{3+} content, the measured photoluminescence lifetimes at 550 and 1196 nm are not affected but upsurges slightly. This confirms that OH- concentration is not affected by the visible and NIR photoluminescence emission property, suggesting energy transfer from these transition levels to OH- is inefficient. The optical properties of RE^{3+} doped barium fluorotellurite glasses are attractive for developing NIR fibre laser around 1200 nm wavelength.

CRediT authorship contribution statement

Eric Kumi Barimah: Conceptualization, Project administration, Experiments, Investigation, Formal analysis, Writing–original draft, Review & Editing; **Yan Chen:** Synthesis of the glasses and characterisation; **Geeta Sharma**: Glass characterisations; **Animesh Jha:** Conceptualization, Funding Acquisition, Review & Editing.

Declaration of competing interest

The authors declare that they have no known competing financial interests or personal relationships that could have appeared to influence the work reported in this paper.

Acknowledgement

References:

1. H.P. V. Do, V.X. Quang, V.P. Tuyen, L.D. Thanh, N. M. Khaidukov, V. N. Makhov, N. T. Thanh, Sensitization of luminescence from Sm^{3+} ions in fluoride hosts K_2YF and K_2GdF_5 by doping with Tb^{3+} ions, J. Lumin., 209(2019) 340-345.

2. V.P. Tuyen, V.X. Quang, P.V. Do, L.D. Thanh, N.X. Ca, V.X. Hoa, L.V. Tuat, L.A. Thi, M. Nogami, An in-depth study of the Judd-Ofelt analysis, spectroscopic properties and energy transfer of Dy^{3+} in alumino-lithium-telluroborate glasses, J. Lumin., 210 (2019) 435-443

3. E. Kumi-Barimah, Y. Chen, R. Tenwick, M. Al-Murish, G. Sherma, A. Jha, Effect of Yb^{3+} on the Structural and Visible to Near-Infrared Wavelength Photoluminescence Properties in Sm^{3+}-Yb^{3+}-Codoped Barium Fluorotellurite Glasses. Materials, *15(*2022*)* 3314.

4. E. Kumi-Barimah, Laser-induced Fluorescence Spectroscopy for applications in chemical sensing and optical refrigeration, PhD thesis (2014).

5. P. X. Le, N. M. Ty, J. Qiu, D. Zhou, H. K. Dan, Enhanced upconversion and near-infrared emissions of co-doped Ho^{3+}/Yb^{3+} in TeO_2-ZnO-Na_2CO_3-La_2O_3 tellurite glasses, Optical Materials Express, 9(10) (2019) 3998-4008.

6. A. Li, Y. Dong, S. Wang, S. Jia, G. Brambilla, P. Wang, Infrared-laser and upconversion luminescence in Ho^{3+}-Yb^{3+} codoped tellurite glass microsphere, J. of Luminescence, 218 (2020) 116826.

7. O. Bentouila, K.E. Aiadi, F. Reheouma, M. Poulain, F. Benhirech, Thermal stability and spectroscopy of Ho^{3+}:Yb^{3+} codoped fluorophosphate glasses, J. of KingSaud University- Science, 31(4) (2019) 628-634.

8. M. Azam, D. K. Mohanty, V. K. Rai, K. Singh, Luminescence and Judd-Ofelt study of Ho^{3+}/Ho^{3+}-Yb^{3+} doped/codoped lead tellurite glasses for multifunctional applications, J. of Luminescence, 239 (2021), 118329.

9. S. Liu, X. Zhu, G. Zhu, K. Balakrishnan, J. Zong, K. Wiersma, A. Chavez-Pirson, R. A. Norwood, N. Peyghambarian, Graphene Q-switched Ho^{3+}-doped ZBLAN fiber laser at 1190 nm, **Optics Letters**, 40 (2) (2015)147-150.

10. S. Wang, Z. Jia, C. Yao, C. He, G. Qin, W. Qin, Ho^{3+}/Yb^{3+} co-doped Tellurite glasses and fibers for 1.2 µm laser applications, WT4A.25, https://doi.org/10.1364/WSOF.2015.WT4A.25

11. B. Richards, S. Shen, A. Jha, Y. Tsang, D. Binks; Infrared emission and energy transfer in Tm3+, Tm^{3+}-Ho^{3+} and Tm^{3+}-Yb^{3+}-doped tellurite fibre, Optics Express 15 (11) (2007) 6546-6551.

12. Y. Tsang, B. Richards, D. Binks, J. Lousteau, A. Jha; A Yb^{3+}/Tm^{3+}/Ho^{3+} triply-doped tellurite fibre laser, , Optics Express 16 (14) (2008) 10690-10695.

13. Y.Tsang, B. Richards, D. Binks, J. Lousteau, A. Jha, Tm^{3+}/Ho^{3+} codoped tellurite fibre laser, , Optics letters 33 (11), (2008)1282-1284.

14. F. Fusari, A.A. Lagatsky, G .Jose, S. Calvez, A. Jha, M. D. Dawson, J. A. Gupta, Femtosecond mode-locked Tm^{3+} and Tm^{3+}-Ho^{3+} doped two µm glass lasers, Optics express 18 (21), 22090-22098 (2010)

15. C.A. Evans, Z .Ikonić, B. Richards, P. Harrison, A. Jha; Numerical Rate Equation Modeling of a 2.1micrometer Tm^{3+}-Ho^{3+} Co-Doped Tellurite Fiber Laser, Journal of Lightwave Technology 27 (19) (2009) 4280-4288

16. C.A .Evans, Z. Ikonic, B. Richards, P Harrison, A.Jha, Numerical Rate Equation Modeling of~ 2.1 µm Tm3+ laser, (2009)

17. Ei Ei Brown, Zackery Fleischman, Jason McKay, and Mark Dubinskii, Optical Spectroscopy of Low-Phonon, Holmium-Doped Barium Fluoride (BaF2) Single Crystals, ARL-TR-9052, 2020.

18. M. Azam, V. K. Rai, Ho^{3+}-Yb^{3+} codoped tellurite based glasses in visible lasers and optical devices: Judd-Ofelt analysis and frequency upconversion, Solid State Sciences, 68(2017) 7-15.

19. S. Wang, C. Li, C. Yao, S. Jia, Z. Jia, G. Qin, W. Qin, Ho^{3+}/Yb^{3+} co-doped TeO$_2$-BaF$_2$-Yb$_2$O$_3$ glasses for ~1.2 mm laser applications, Optical Materials,64(2017) 421-426.

20. I. Kamma, B. R. Reddy, Energy upconversion in holmium doped lead–germano–tellurite glass, J. of Applied Physics 107(2010) 113102.

21. Gouveia-Neto A.S., Da Costa E.B, Bueno L.A, Ribeiro S.J.L, Intense red upconversion emission in infrared excited holmium-doped PbGeO$_3$-PbF$_2$-CdF$_2$ transparent glass ceramic, *Journal of Luminescence*, 110 (1-2)(2004)79 – 84.

22. F. Reichert, F. Moglia, P. W. Metz, A. Arcangeli, D.-T. Marzahl, S. Veronesi, D. Parisi, M. Fechner, M. Tonelli, and G. Huber, Prospects of Holmium-doped fluorides as gain media for visible solid-state lasers, Optical Materials Express, 5(1) (2015) 88-101.

23. Y. Yan, A. J. Faber, H. de Waal, Luminescence quenching by OH groups in highly Er-doped phosphate glasses, Journal of Non-Crystalline Solids 181 (1995) 283-290.

24. D. K. Mohantya, V. K. Rai, Y. Dwivedi, Yb^{3+} sensitized Tm^{3+} upconversion in tellurite lead oxide glass, Spectrochimica Acta Part A, 89 (2012) 264–267

25. M. Khalid, D. G. Lancaster, H. Ebendorff-Heidepriem, Spectroscopic analysis and laser simulations of Yb^{3+}/Ho^{3+} co-doped lead-germanate glass, Optical Materials Express, 10(11) (2020)2819-2833

26. B.M. Walsh, Advances in spectroscopy for laser and sensing: Judd-Ofelt theory-priniciples and practices, springer, (2006) 403-433

27. B.M. Walsh and N.P. Barnes, Branching ratios, cross sections, and radiative lifetimes of rare earth ions in solids : application to Tm^{3+} and Ho^{3+} ions in LiYF$_4$, J. Appl. Phys., 83 (5) (1998), 2772-2787.

28. P.R. Watekar, S. Ju, W-T Han, Optical properties of Ho-doped germano-silica glass optical fiber, Journal of Non-crystalline solid, 354 (2008) 1453-1459.

29. E. Kolobkova, A. Alkhlef, A. Yasukevich, A. Babkina, spectroscopic and lasing properties of Er3+/Yb3+ doped fluorophosphate glass with small additives of phosphates, Optical materials express, 9(9) (2019) 3666-3678.
30. L. L. Fluyt, A. Ceulemans, W.T. Carnall, Magnetic dipole transitions as standards for Judd-Ofelt parametrization in lanthanide spectra, J. Chem. Phys., 95 (1991), 3-10
31. R. Peacock, The intensities of lanthanide f-f transitions, Struct. Bond., 22 (1975) 83
32. I. Pal, A. Agarwal, S. Sanghi, M. Aggarwal, S. Bhardwaj, Fluorescence and radiative properties of Nd^{3+} ions doped zinc bismuth silicate glasses, J. Alloys Compd., 587 (2014) 332338
33. M. Venkateswarlu , Sk. Mahamuda , K. Swapna , M.V.V.K.S. Prasad, A. Srinivasa Rao, Suman Shakya, A. Mohan Babu, G. Vijaya Prakash, Holmium doped Lead Tungsten Tellurite glasses for green luminescent applications, Journal of Luminescence 163(2015), 64-71.
34. V. M. Villacampa, V. M Orera, R. I. Merino, R. Cases, P. J. Alonso, and R. Alcala, Optical properties of ZnF_2-CdF_2 glasses doped with 4f ions, Mater. Res. Bull. 26(1991) 741.
35. N. Rakov, G. S. Maciel, and C. B. de Araujo, Energy transfer assisted frequency upconversion in Ho^{3+} doped fluoroindate glass, J. Appl. Phys. 91(2002) 1272.
36. S. Dai, C. Yu, G. Zhou, J. Zhang, G. Wang, L. Hu, Concentration quenching in erbium-doped tellurite glasses, Journal of Luminescence, 117(2006) 39-45.
37. S. Dai, C. Yu, G. Zhou, J. Zhang, G. Wang, L. Hu, Effect of hydroxyl groups on nonradiative decay of Er^{3+}: $^4I_{13/2} \rightarrow ^4I1_{5/2}$ transition in zinc tellurite glasses, Materials Letters, 59(2005) 2333-2336.
38. S. Balaji, A. D. Sontakke, R. Sen, A. Kalyandurg, Efficient ~2.0 µm efficiency from Ho^{3+} doped tellurite glass sensitised by Yb^{3+} ions: Judd-Ofelt analysis and energy transfer mechanism, Optical materials express, 1(2) (2011)138-150.